Journal Pre-proof

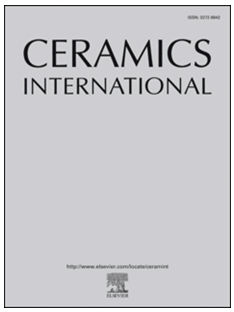

A kinetic study of $La_{0.75}Sr_{0.25}Cr_{0.5}Mn_{0.5}O_{3-\delta}$ nano-structured electrodes for intermediate temperature symmetric solid oxide fuel cells

Alejandra Montenegro-Hernández, Corina M. Chanquía, Liliana V. Mogni

PII: S0272-8842(23)03314-X

DOI: https://doi.org/10.1016/j.ceramint.2023.10.243

Reference: CERI 38383

To appear in: *Ceramics International*

Received Date: 23 August 2023

Revised Date: 12 October 2023

Accepted Date: 23 October 2023

Please cite this article as: A. Montenegro-Hernández, C.M. Chanquía, L.V. Mogni, A kinetic study of $La_{0.75}Sr_{0.25}Cr_{0.5}Mn_{0.5}O_{3-\delta}$ nano-structured electrodes for intermediate temperature symmetric solid oxide fuel cells, *Ceramics International* (2023), doi: https://doi.org/10.1016/j.ceramint.2023.10.243.

This is a PDF file of an article that has undergone enhancements after acceptance, such as the addition of a cover page and metadata, and formatting for readability, but it is not yet the definitive version of record. This version will undergo additional copyediting, typesetting and review before it is published in its final form, but we are providing this version to give early visibility of the article. Please note that, during the production process, errors may be discovered which could affect the content, and all legal disclaimers that apply to the journal pertain.

© 2023 Published by Elsevier Ltd.

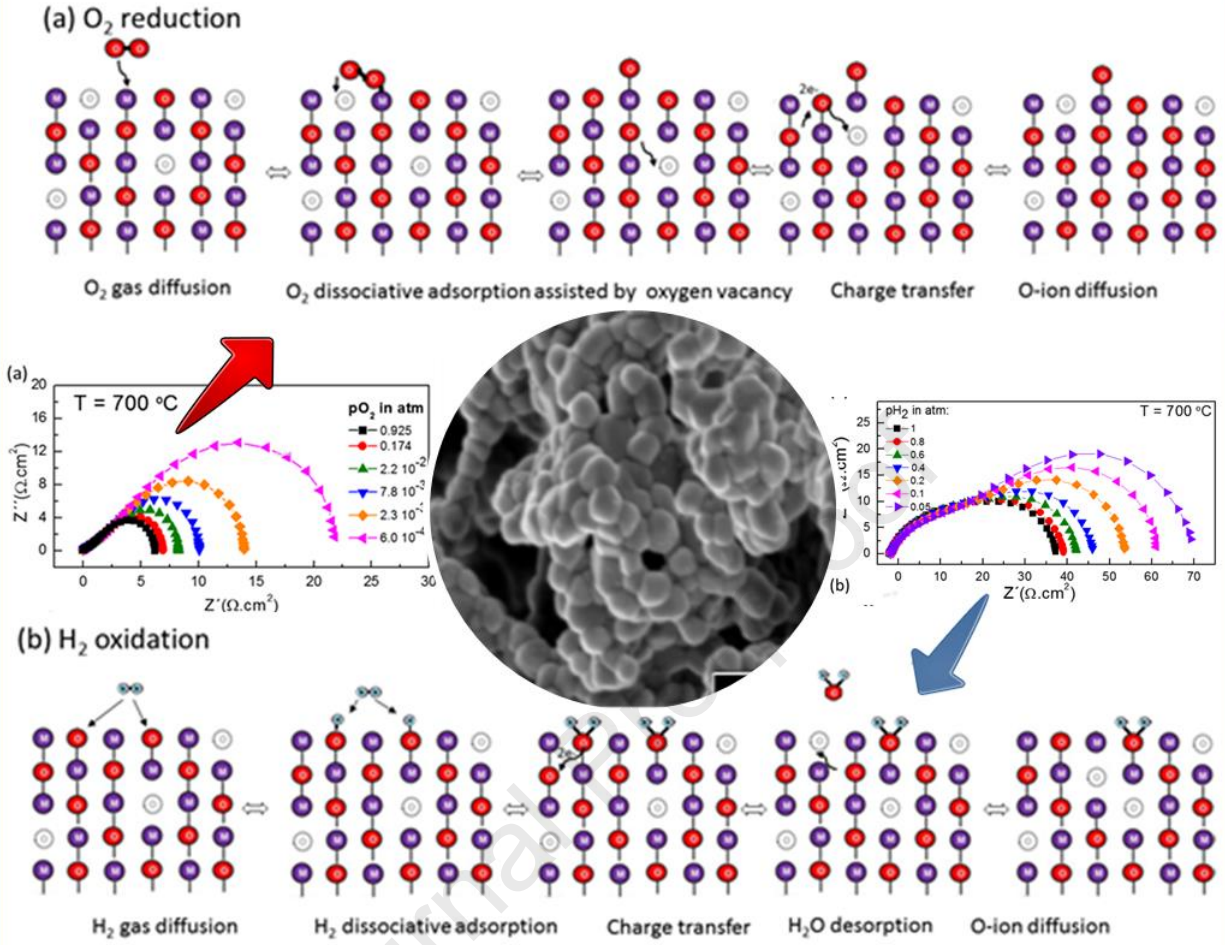

Schematic illustration of the (a) O_2 reduction and (b) H_2 oxidation, including: O_2 or H_2 gas diffusion, O_2 or H_2 dissociative adsorption on the oxide electrode surface; charge transfer reaction forming O-ion or H_2O molecule; desorption of H_2O from the oxide surface; and oxygen ion diffusion.

Journal Pre-proof

A kinetic study of $La_{0.75}Sr_{0.25}Cr_{0.5}Mn_{0.5}O_{3-\delta}$ nano-structured electrodes for intermediate temperature symmetric solid oxide fuel cells.

Alejandra Montenegro-Hernández[a,b], Corina M. Chanquía[a,b] and Liliana V. Mogni[a,b,c]

[a] *Departamento Caracterización de Materiales-Gerencia de Investigación Aplicada-Instituto de Nanociencias y Nanomateriales, Centro Atómico Bariloche - Comisión Nacional de Energía Atómica (CAB-CNEA), Av. Ezequiel Bustillo 9500, R8402AGP, San Carlos de Bariloche, Argentina.*

[b] *Consejo Nacional de Investigaciones Científicas y Técnicas (CONICET), Avenida Rivadavia 1917, C1033AAJ, Ciudad Autónoma de Buenos Aires, Argentina.*

[c] *Instituto Balseiro, Universidad Nacional de Cuyo, Av. Ezequiel Bustillo 9500, R8402AGP San Carlos de Bariloche, Río Negro, Argentina.*

*Corresponding author: alejandra.montenegro@gmail.com

Journal Pre-proof

Journal Pre-proof

Abstract

$La_{0.75}Sr_{0.25}Cr_{0.5}Mn_{0.5}O_{3-\delta}$ (LSCM) mixed conducting has been studied as nanostructured air and fuel electrode, for intermediate temperature symmetric Solid Oxide Fuel cell (S-SOFC). The possible mechanisms involved in the oxygen reduction and hydrogen oxidation reactions of these LSCM nanostructures porous electrodes deposited on $La_{0.8}Sr_{0.2}Ga_{0.8}Mg_{0.2}O_{3-\delta}$ (LSGM) electrolyte, were analyzed by electrochemical impedance spectroscopy (EIS) at 700 °C varying the oxygen partial pressure (pO_2) and the hydrogen partial pressure (pH_2). This analysis was complemented by the study of the electrical conductivity by the four-probe DC technique in the range between 300 and 800 °C in flowing dry atmospheres of air or H_2. Results suggested that the O_2 reduction reaction mechanism involves the O_2- dissociative adsorption and O- ion migration near the surface region, while the H_2-oxidation reaction limiting-step is controlled by a slow charge transfer process, and H_2- dissociative adsorption on the ultimate O-layer.

Keywords: S-SOFC; chromite, manganite; nano- structured; EIS

Journal Pre-proof

Introduction

Replace conventional energy sources with alternative and environment-friendly energy sources, has led the transition to a reduced carbon emission energy system. In this sense, fuel cell technologies have emerged as an important alternative using the chemical energy of light fuels such as hydrogen, methane, methanol, etc, to produce clean and efficient electricity by electrochemical conversion. Among fuel cell devices, solid oxide fuel cells (SOFCs) have proven to be highly efficient, because they can utilize high quality heat produced in co-generation to increases the efficiency of power conversion systems [1].

Also, the high temperature of operation allows using low cost raw materials such as oxides to replacing high cost precious metal as electrocatalyst. However, Cells of SOFCs are involves three basic components a porous anode, a dense electrolyte, and a porous cathode. Each element requires materials with specific characteristics in terms of their transport and electrocatalytic properties, thermodynamic stability and microstructure [2,3]. The traditional materials used in the SOFCs cells operate in the temperature range between 800 and 1000 °C, this make o~~O~~ne of the major drawbacks of SOFCs is their high operating temperature which leads to some serious problems such as chemical degradation [4,5], mainly at the interface between the cell components [6–8]. In the last years, a new concept of symmetrical SOFCs (S-SOFCs), where the same materials are employed as both oxygen and fuel electrodes, has obtained a significant interest with a view to reduce some disadvantages of the traditional SOFCs [9–11]. With this kind of design, the manufacturing process, especially the requirement of thermal treatments, can be simplified, reducing fabrication costs and incompatibility problems due to chemical reactivity at the interface between the cell components. The S-SOFC demands an adequate electrode stable in both, anode and cathode atmospheres that complies with certain features such as electrochemical activity, structure stability, and compatibility with electrolyte materials under reducing and oxidizing atmospheres [12–16]. It is well known that Ni/YSZ cermet is the most commonly used anode material in SOFCs [17]. However, such cermets present some disadvantages like low tolerance to sulfur, carbon deposition when using hydrocarbon fuels, and volume instability upon redox cycling in a high-temperature oxidizing environment [18–21]; therefore, conventional electrodes are not suitable for use as symmetrical electrodes. However, most of these problems have been overcome with the introduction of new materials. In this sense, $La_{0.75}Sr_{0.25}Cr_{0.5}Mn_{0.5}O_{3-\delta}$ (LSCM) perovskite has demonstrated a

promising combination of properties for its employ as anode and cathode in SOFC devices [14,22–28]. The LSCM perovskite has excellent chemical stability in both oxidizing and reducing environments [29,30], and also demonstrated its versatility for use as an anode running on direct natural gas feed [28], which could reduce the cost by simplifying the device's design by dispensing of external reformer. Additionally this material presents catalytic activity able to oxidize methane fuel without steam, low carbon deposition, and high durability against sulfur poisoning [31]. On the other hand, has been reported by different authors that LSCM material can also be used as an efficient cathode [29,32,33]. All these characteristics make that the LSCM a strong attraction to be a promising symmetrical electrode.

In our previous works, we present the synthesis by combustion of pure phase LSCM nanocrystallites [34], and the bottom-up building process of nanostructured LSCM electrodes by employing $La_{0.8}Sr_{0.2}Ga_{0.8}Mg_{0.2}O_{3-\delta}$ (LSGM) as electrolyte [28]. In this work, a systematic characterization of the electrochemical performance of LSCM as both, anode and cathode material by electrochemical impedance spectroscopy (EIS) and four-probe DC technique is presented. To the best of our knowledge, the present work is the first to report an electrode kinetics study of nanostructured LSCM material varying the oxygen (pO_2) and hydrogen (pH_2) partial pressures.

Experimental section.

Nanostructured powders of $La_{0.75}Sr_{0.25}Cr_{0.5}Mn_{0.5}O_{3-\delta}$ (LSCM) composition were prepared by combustion synthesis, their main morphological and structural characteristics have been presented and discussed by us elsewhere [28]. In this work the LSCM were process to

obtain dense sample for electrical conductivity tests and porous electrodes for electrochemical characterization. The LSCM samples were characterized by Scanning Electronic Microscopy (SEM) using a SEM-FEG Nova Nano SEM 230 microscope and X Ray Diffraction (XRD) using a PANalytical θ/θ Bragg-Brentano Empyrean diffractometer with Cu ($K_{\alpha1}$+$K_{\alpha2}$) radiations and graphite monocromator.

Total electrical conductivity of LSCM was performed by four-probe DC technique; the obtained powders were pressed into pellets and sintered at 1350 °C for 4 h with heating rate of 5 ºC/min. The sintered samples with ~95% relative density were cut by using a diamond saw into bars 0.8×0.3 ×0.3 cm. Four Pt wires were putted each bar and bonded to the sample using Pt paste, and then the samples were heated to 800 °C to sinter the conducting paste. Four-point DC conductivity measurements were performed by using an Agilent 3497A scanner-multimeter by sending a current through the wires at the ends of the bars and then measuring the voltage drop across and two middle wires. The sample was heated, in flowing dry atmospheres of air or H_2, to desired temperature in the range between 300 and 800 °C. Once the temperature stabilized, the conductivity was monitored until a stable value was reached. Afterwards, the electrical conductivity was measured by cooling in both atmospheres. The data acquisition was performed using a LabView program.

The electrochemical characterization of porous LSCM nanoelectrodes was achieved by Electrochemical Impedance Spectroscopy (EIS). This characterization was carried out on dense $La_{0.9}Sr_{0.1}Ga_{0.8}Mg_{0.2}O_{2.85}$ (LSGM) as electrolyte, which was prepared by sintering LSGM powder at 1450 °C for 4 h. Inks for electrode deposition were prepared using LSCM nano-powder (35 wt. %) synthesized by us by employing the combustion method [28], polyvinyl butyral (2 wt. %), polyethyleneglycol (1 wt. %), ethanol (30 wt. %) and α-

terpineol (27 wt. %), which were then deposited onto both surfaces of the LSGM electrolyte by spin coating technique. Subsequently, the cells were placed and maintained during 10 min in a preheated furnace at 1000 °C. EIS measurements were performed with a frequency response analyzer (FRA) coupled to an AUTOLAB-PGSTAT32 potentiostat, measuring between 0.2 mHz and 1 MHz, with 50 mV of amplitude and 0 V of bias potential. The EIS spectra were collected at 700 °C varying the oxygen partial pressure (pO_2) between 1 and 6 $x10^{-4}$ atm and the hydrogen partial pressure (pH_2) between 1 and 5 $x10^{-2}$ atm. Controlled pO_2 atmospheres were provided by an electrochemical system composed of an oxygen pump and an oxygen sensor [35]. The resulting spectra were fitted with Electrical Equivalent Circuit using Zview program.

Results and discussion

Figure 1 (a) shows the both conductivity data as a function of temperature, in air and 10% H_2/Ar dry atmospheres. The conductivity in air is at least on order of magnitude higher than in H_2/Ar for all temperature range, suggesting a p-type semiconducting behavior (see Table 1). Note that, in the samples prepared for electrical characterization, high temperature of sintering increases the grain sizes and guarantee a good grain interconnection (Fig. 1 (b)). According to Delahaye et al., the diminution of the conductivity in $La_{0.75}Sr_{0.25}Cr_{0.5}Mn_{0.3}Ni_{0.2}O_{3-\delta}$ sample under reducing atmosphere will be related to the mixed valence of manganese Mn^{3+}/Mn^{4+} [36]. Therefore, in LSCM it is reasonable to assume that also the total number of carrier decreases due to Mn^{4+} reduction, leading to the total conductivity drop. In addition, the conductivity has a thermally activated behavior, increases at higher temperature reaching values around ~12 and 0.5 Scm^{-1} at 800 °C in air and H_2, respectively. The conductivities values obtained in reducing atmosphere are

comparable to those reported for other perovskite (e.g. $Sr(Ti,Fe)O_3$ [37] and double perovskite (e.g. $SrMgMoO_6$ [38–41])type anodes. The activation energy (E_a) in the temperature range between 300 and 800 °C was around 0.19 and 0.44 eV under air and 10% H_2/Ar atmosphere, respectively. The higher activation energy observed in hydrogen suggests that the high reduction of the electrical conductivity as temperature is reduced could increase the ohmic loss in the S-SOFC cells.

Fig. 2 (a) and (b) present SEM images of the top view and the cross-section of the LSCM-electrode deposited on LSGM electrolyte and treated at 1000 °C for 10 min. The LSCM-electrode shows porous microstructures with good interconnectivity between nanocrystallites, electrode thickness ~ 30 μm, crystallite size ~ 100 nm and specific surface area ~ 5.3 m^2/g [28]. The LSCM-electrode presented an adequate adherence to the LSGM electrolyte, and not significant changes were observed in the electrode/electrolyte interfaces after the electrochemical tests. Also, the XRD pattern of the electrode surface shows only peaks correspondents to $La_{0.75}Sr_{0.25}Cr_{0.5}Mn_{0.5}O_{3-\delta}$ phase (see Fig. 2 (c)), which are characteristic of trigonal/ rhombohedral R-3c space group [24].

LSCM was evaluated as potential SOFC cathode and anode using EIS measurements. The analysis of the evolution of EIS spectra with the concentration of active species, O_2 and H_2 for cathode and anode reaction, respectively, helps to understand the limiting-steps of the electrochemical reaction and to design materials strategies to reduce electrode polarization resistances. Fig. 3 (a) and (b) show the evolution of the EIS Nyquist and Bode spectra, respectively, collected at 700 °C as a function of pO_2. The shape of the spectra shows the overlapping of at least two contributions to the EIS spectra, suggesting that the mechanism limiting the oxygen reduction reaction (ORR) is controlled at least by two

steps. In order to identify which mechanism is controlling the ORR, the spectra obtained were fitted using an equivalent electrical circuit. In all cases, an inductive element (L) due to the inductance of the wires in series with an ohmic resistance R-el that corresponds mainly to the electrolyte resistance was included. The best fitting was obtained by using a Warburg-type (Z_W) element for the high frequencies contribution and a combination of one resistance in parallel with one constant phase element (R_{LF}//CPE_{LF}) for the low frequency contribution.

Fig. 3 (c) shows the evolution with pO_2 at 700 °C of the cathode polarization resistance for Warburg element ($R_{W,C}$) and the low frequency contribution ($R_{LF,C}$). For each step, there is a relation between the polarization resistances and pO_2 values, $R \sim pO_2^n$ where, "n" is characteristic of the nature of the process. In Table 1 are listed some relevant parameters obtained from the fit of the EIS spectra collected. The HF contribution is independent of the pO_2 ($n \approx 0$) and presents a pseudo-capacitances values around 10^{-2} Fcm^{-2}. Adler approach yields that capacitance values within the range 10^{-3} – 10^{-2} Fcm^{-2} are representative of surface processes while a semi-infinite Warburg behavior is consistent with oxygen bulk diffusion [42]. Then, it can be assumed that the HF contribution is due to O-ionic diffusion and it is limited to the near surface region. On the other hand, the obtained values of capacitance around 10^{-2} Fcm^{-2} and pO_2 dependence close to 0.5 suggest that O_2-dissociative adsorption is the rate-limiting step of the low frequency contribution.

The ORR mechanism is close related to the role of the O-vacancies on the oxygen incorporation into mixed conducting perovskites. In this sense, M. M. Kuklja et. al performed a comparative discussion, based on theoretical and experimental information, about the mechanism of O_2-reduction for three different kind of materials: $(La,Sr)MnO_3$ (LSM), $(La,Sr)(Co,Fe)O_3$ (LSCF) and $(Ba,Sr)(Co,Fe)O_3$ (BSCF) [43]. They proposed that

the individual reaction steps for the oxygen incorporation can take place with or without a vacancy being actively involved [43]. In the case of LSM electrode, M. M. Kuklja et. al suggested that, due to the low oxygen vacancies concentration, the O_2 is adsorbed on the transition metal and the dissociation is assisted by the O-vacancies. Besides, due to the good electrical conductivity of LSM, the electron transfer processes are faster than the other reaction steps, therefore, the authors suggested that the O_2-reduction in LSM is limited either the ion motion or the bond breaking [43]. Taking into account the similarity between LSM and LSCM, the good electrical conductivity of LSCM under air (see Fig. 1), the poor O-ion conductivity (σ_O) under oxidative atmosphere [44], and the dependence of the electrode resistance with the pO_2, it is reasonable to assume that the ORR on the LSCM cathode is in agreement with the mechanism proposed by M. M. Kuklja et. al for the LSM [43]. In this case, the limiting step is the O_2-dissociative adsorption and the O-ion migration in the near surface region.

Fig. 4 (a) and (b) show the EIS Nyquist and Bode spectra collected at 700 °C as a function of pH_2. Similarly to the cathodic behavior, the pH_2 evolution of the EIS spectra suggests the presences of two processes. The equivalent electrical circuit is conforming by an inductive element due to the inductance of the wires in series with a resistance that corresponds to the electrolyte resistance. In this case, the high and low frequency arcs were fitted with a combination of one resistance in parallel with one constant phase element (R_{HF}//CPE_{HF} and R_{LF}//CPE_{LF}). Fig. 4 (c) shows the log-log plot of the anodic polarization resistances vs. pH_2 at 700 °C and the table 1 shows some relevant parameters obtained from the fit. The capacitance values of both contributions are one order of magnitude lower than those found in air, suggesting a more surface character of the anodic process. The polarization resistance of the HF contribution is independent of the partial pressure of the

active specie ($R_{HF,A} = pH_2^0$), while LF resistance varies with ($R_{LF,A} = pH_2^{-0.37}$). In this sense, the information related to the HOR mechanism in perovskite-type anodes is quite limited. For example, Zhu et. al. studied $Sr(Ti_{0.3}Fe_{0.7})O_3$ (STF) perovskite as S-SOFC electrode by varying pH_2 in the anode side (keeping the cathode side in air). They found that EIS spectra has also two contributions, but whereas the resistances of the LF arc, that varies with $pH_2^{-0.5}$, was assigned to the activated dissociative hydrogen adsorption process, the resistances of the HF arc, which is also pH_2 independent, was assigned to the cathodic contributions [45]. For the LSCM, it can be assumed that the HF arc, which is pH_2-independent (see Figure 4), must be assigned to some H_2-oxidation limiting step, while the LF arc has a $\sim pH_2^{0.5}$ and their capacitance values, would indicate a surface process associated to the H_2-disociative adsorption on the ultimate O-layer. The increases of the O-ionic transport under reducing condition reported by Kharton et al. [44], and the decreases of the electrical conductivity observed here (see Figure 1 and Table 1), allow us to assume a major control of the charge-transfer process and a lower limitation of O-ion diffusion for the LSCM working as anode. These considerations are in agreement with the Mars–van–Krevelen (MVK) mechanism presented for SOFC anodes by McIntosh and van den Bossche [46]. In the MVK mechanism, the reaction occurs via the reduction and oxidation (redox) of lattice oxygen sites of the electrocatalyst. The reduction occurs via fuel oxidation at the active surface site, accompanied by a two electron charge transfer. Re-oxidation occurs by bulk ion transport (i.e. oxygen diffusion). [47].

According to the discussed above, the mechanism of electrode reaction for LSMC electrodes can be proposed as (see Fig. 5):

(i) The O_2-reduction taking place through a mechanism where the O_2 is adsorbed either on a surface M-site (M = Mn and Cr) or on a O-vacancy site and then dissociated through a

vacancy assisted-mechanism ($R_{LF,C} \sim pO_2^{0.5}$), followed by a fast charge transfer process (σ_{el}= 8.95Scm^{-1}) and a controlling O-ion diffusion ($R_{W,C} \sim pO_2^{0}$ at 700°C and σ_O ~3.10^{-5} Scm^{-1} in air at 950°C [44]) in the near surface zone.

(ii) The H_2-oxidation running by an activated dissociative H_2-adsorption process on the O-external layer ($R_{LF,A} = pH_2^{-0.5}$), followed by a slow charge transfer process ($R_{HF,C} \sim pO_2^{0}$ and σ_{el} ~0.3 Scm^{-1}) and a fast H_2O desorption and O-ion diffusion (σ_O ~30.10^{-5} Scm^{-1} in H_2 at 950°C [8]) to fill the empty H_2O surface site.

Conclusions

The study of the electrochemical performance of $La_{0.75}Sr_{0.25}Cr_{0.5}Mn_{0.5}O_{3-\delta}$ by EIS by using LSGM as the electrolyte, and their electrical conductivity by four-probe DC technique allows to obtain original information about the mechanisms involved in the oxygen reduction and hydrogen oxidation reactions of these porous nanostructured electrodes of SOFC devices. The EIS spectra recorded by varying the pO_2 and pH_2 were fitted by using an EEC. The best fit results were obtained with the EEC composed of an inductive element, an ohmic resistance, and two circuits: in air a high frequency Warburg in series with a parallel combinations of one resistance and one constant phase element (R//CPE); and in hydrogen two R//CPE circuits in series. For O_2 reduction reaction (ORR), the W-high frequency is related to O-ionic diffusion limited to the near surface region, while the R//CPE element of low frequency is related to O_2- dissociative adsorption and O- ion migration near surface region.

In the case of H_2 oxidation reaction (HOR), the HF arc can be assigned to some H_2-oxidation limiting-step controlled by a slow charge transfer process, while the LF arc would be limited to a surface process associated to the H_2-disociative adsorption on the ultimate

O-layer. This study, in addition to provide possible mechanisms involved in the oxygen reduction and hydrogen oxidation reactions of these porous nanostructured electrodes, also it proposes that the nanocrystalline LSCM perovskite -synthesized by combustion method- could be used as precursor to build electrodes in S-SOFCs operating up to 700°C.

Acknowledgments

This work was financially supported by Comisión Nacional de Energía Atómica (CNEA), Consejo Nacional de Investigaciones Científicas y Técnicas (CONICET PIP 067595) and Agencia Nacional de Promoción de Ciencia y Tecnología (ANPCyT PICT 2019-03721).

References

[1] D.J.L. Brett, A. Atkinson, N.P. Brandon, S.J. Skinner, Intermediate temperature solid oxide fuel cells, Chem. Soc. Rev. 37 (2008) 1568. https://doi.org/10.1039/b612060c.

[2] A. Nakajo, J. Kuebler, A. Faes, U.F. Vogt, H.J. Schindler, L.-K. Chiang, S. Modena, J. Van herle, T. Hocker, Compilation of mechanical properties for the structural analysis of solid oxide fuel cell stacks. Constitutive materials of anode-supported cells, Ceram. Int. 38 (2012) 3907–3927. https://doi.org/10.1016/j.ceramint.2012.01.043.

[3] E. Ivers-Tiffée, A. Weber, D. Herbstritt, Materials and technologies for SOFC-components, J. Eur. Ceram. Soc. 21 (2001) 1805–1811. https://doi.org/10.1016/S0955-2219(01)00120-0.

[4] H. Yokokawa, H. Tu, B. Iwanschitz, A. Mai, Fundamental mechanisms limiting solid oxide fuel cell durability, J. Power Sources. 182 (2008) 400–412.

Journal Pre-proof

https://doi.org/10.1016/j.jpowsour.2008.02.016.

[5] J. Wei, T. Osipova, J. Malzbender, M. Krüger, Mechanical characterization of SOFC/SOEC cells, Ceram. Int. 44 (2018) 11094–11100. https://doi.org/10.1016/j.ceramint.2018.03.103.

[6] M.Z. Khan, R.-H. Song, M.T. Mehran, S.-B. Lee, T.-H. Lim, Controlling cation migration and inter-diffusion across cathode/interlayer/electrolyte interfaces of solid oxide fuel cells: A review, Ceram. Int. 47 (2021) 5839–5869. https://doi.org/10.1016/j.ceramint.2020.11.002.

[7] A. Montenegro-Hernández, A. Soldati, L. Mogni, H. Troiani, A. Schreiber, F. Soldera, A. Caneiro, Reactivity at the Ln2NiO4+/electrolyte interface (Ln = La, Nd) studied by Electrochemical Impedance Spectroscopy and Transmission Electron Microscopy, J. Power Sources. 265 (2014) 6–13. https://doi.org/10.1016/j.jpowsour.2014.04.082.

[8] K.-J. Hwang, M. Shin, M.-H. Lee, H. Lee, M.Y. Oh, T.H. Shin, Investigation on the phase stability of yttria-stabilized zirconia electrolytes for high-temperature electrochemical application, Ceram. Int. 45 (2019) 9462–9467. https://doi.org/10.1016/j.ceramint.2018.09.026.

[9] K. Zhu, B. Luo, Z. Liu, X. Wen, Recent advances and prospects of symmetrical solid oxide fuel cells, Ceram. Int. 48 (2022) 8972–8986. https://doi.org/10.1016/j.ceramint.2022.01.258.

[10] M. Santaya, C.E. Jiménez, H.E. Troiani, E.A. Carbonio, M.D. Arce, L.M. Toscani, R. Garcia-Diez, R.G. Wilks, A. Knop-Gericke, M. Bär, L.V. Mogni, Tracking the nanoparticle exsolution/reoxidation processes of Ni-doped SrTi 0.3 Fe 0.7 O 3− δ electrodes for intermediate temperature symmetric solid oxide fuel cells, J. Mater.

Chem. A. 10 (2022) 15554–15568. https://doi.org/10.1039/D2TA02959F.

[11] Y. Ling, T. Li, Y. Yang, Y. Tian, X. Wang, K. Chen, D. Dong, Y. Chen, K. Amezawa, Oxygen vacancies-rich iron-based perovskite-like electrodes for symmetrical solid oxide fuel cells, Ceram. Int. 47 (2021) 12916–12925. https://doi.org/10.1016/j.ceramint.2021.01.154.

[12] J. Ramírez-Hernández, A.M. Torres-Huerta, S.B. Brachetti-Sibaja, M.A. Domínguez-Crespo, D. Palma-Ramírez, A.E. Rodríguez-Salazar, A. Ezeta-Mejia, La0.7− xLnxCa0.3MnO3(Ln = Pr or Sm) perovskites as electrode materials for SOFCs, Ceram. Int. 48 (2022) 21221–21234. https://doi.org/10.1016/j.ceramint.2022.04.031.

[13] M. Gou, R. Ren, W. Sun, C. Xu, X. Meng, Z. Wang, J. Qiao, K. Sun, Nb-doped Sr2Fe1.5Mo0.5O6-δ electrode with enhanced stability and electrochemical performance for symmetrical solid oxide fuel cells, Ceram. Int. 45 (2019) 15696–15704. https://doi.org/10.1016/j.ceramint.2019.03.130.

[14] S. Tao, J.T.S. Irvine, Phase Transition in Perovskite Oxide La 0.75 Sr 0.25 Cr 0.5 Mn 0.5 O 3- δ Observed by in Situ High-Temperature Neutron Powder Diffraction, Chem. Mater. 18 (2006) 5453–5460. https://doi.org/10.1021/cm061413n.

[15] A. Weber, E. Ivers-Tiffée, Materials and concepts for solid oxide fuel cells (SOFCs) in stationary and mobile applications, J. Power Sources. 127 (2004) 273–283. https://doi.org/10.1016/j.jpowsour.2003.09.024.

[16] G. Wang, W. Wu, W. Guan, L. Jin, W. Guo Wang, Effect of conductivity and adhesive properties of cathode current-collecting layer on cell performance inside stack for planar solid oxide fuel cells, Ceram. Int. 40 (2014) 11023–11030. https://doi.org/10.1016/j.ceramint.2014.03.117.

Journal Pre-proof

[17] S.C.K.K. Singhal;, High-temperature Solid Oxide Fuel Cells: Fundamentals, Design and Applications, 1st ed., Elsevier, Oxford, 2004. https://shop.elsevier.com/books/high-temperature-solid-oxide-fuel-cells-fundamentals-design-and-applications/singhal/978-1-85617-387-2.

[18] S.P. Jiang, S.H. Chan, A review of anode materials development in solid oxide fuel cells, J. Mater. Sci. 39 (2004) 4405–4439. https://doi.org/10.1023/B:JMSC.0000034135.52164.6b.

[19] Y. Matsuzaki, The poisoning effect of sulfur-containing impurity gas on a SOFC anode: Part I. Dependence on temperature, time, and impurity concentration, Solid State Ionics. 132 (2000) 261–269. https://doi.org/10.1016/S0167-2738(00)00653-6.

[20] Y. ZHANG, B. LIU, B. TU, Y. DONG, M. CHENG, Redox cycling of Ni–YSZ anode investigated by TPR technique, Solid State Ionics. 176 (2005) 2193–2199. https://doi.org/10.1016/j.ssi.2005.06.016.

[21] B. STEELE, Oxidation of methane in solid state electrochemical reactors, Solid State Ionics. 28–30 (1988) 1547–1552. https://doi.org/10.1016/0167-2738(88)90417-1.

[22] Tao, J.T.S. Irvine, S.M. Plint, Methane Oxidation at Redox Stable Fuel Cell Electrode La 0.75 Sr 0.25 Cr 0.5 Mn 0.5 O 3- δ, J. Phys. Chem. B. 110 (2006) 21771–21776. https://doi.org/10.1021/jp062376q.

[23] S. He, H. Dai, X. Chen, Q. Shi, Z. Tao, Investigation of La0.75Sr0.25Cr0.5Mn0.5O3-δ–Ag composite anodes for solid oxide fuel cells obtained via a low-temperature sintering process, Ionics (Kiel). 26 (2020) 6225–6232. https://doi.org/10.1007/s11581-020-03750-y.

[24] Z. Ma, Y. Li, Y. Zheng, W. Li, X. Chen, X. Sun, X. Chen, J. Zhou, La0.75Sr0.25Cr0.5Mn0.5O3- as cathode for electrolysis and co-electrolysis of CO2

and H2O in solid oxide electrolysis cell, Ceram. Int. 47 (2021) 23350–23361. https://doi.org/10.1016/j.ceramint.2021.05.049.

[25] J. Meng, N. Yuan, X. Liu, C. Yao, Q. Liang, D. Zhou, F. Meng, J. Meng, Synergistic Effects of Intrinsic Cation Disorder and Electron-Deficient Substitution on Ion and Electron Conductivity in La 1– x Sr x Co 0.5 Mn 0.5 O 3−δ (x = 0, 0.5, and 0.75), Inorg. Chem. 54 (2015) 2820–2829. https://doi.org/10.1021/ic502989c.

[26] K.M. Papazisi, S. Balomenou, D. Tsiplakides, Synthesis and characterization of La0.75Sr0.25Cr0.9M0.1O3 perovskites as anodes for CO-fuelled solid oxide fuel cells, J. Appl. Electrochem. 40 (2010) 1875–1881. https://doi.org/10.1007/s10800-010-0150-6.

[27] F.M. Sapountzi, S. Brosda, K.M. Papazisi, S.P. Balomenou, D. Tsiplakides, Electrochemical performance of La0.75Sr0.25Cr0.9M0.1O3 perovskites as SOFC anodes in CO/CO2 mixtures, J. Appl. Electrochem. 42 (2012) 727–735. https://doi.org/10.1007/s10800-012-0459-4.

[28] C.M. Chanquía, A. Montenegro-Hernández, H.E. Troiani, A. Caneiro, A bottom-up building process of nanostructured La0.75Sr0.25Cr0.5Mn0.5O3-δ electrodes for symmetrical-solid oxide fuel cell: Synthesis, characterization and electrocatalytic testing, J. Power Sources. 245 (2014). https://doi.org/10.1016/j.jpowsour.2013.06.124.

[29] D.M. Bastidas, S. Tao, J.T.S. Irvine, A symmetrical solid oxide fuel cell demonstrating redox stable perovskite electrodes, J. Mater. Chem. 16 (2006) 1603. https://doi.org/10.1039/b600532b.

[30] J.C. Ruiz-Morales, J. Canales-Vázquez, J. Peña-Martínez, D.M. López, P. Núñez, On the simultaneous use of La0.75Sr0.25Cr0.5Mn0.5O3−δ as both anode and

Journal Pre-proof

cathode material with improved microstructure in solid oxide fuel cells, Electrochim. Acta. 52 (2006) 278–284. https://doi.org/10.1016/j.electacta.2006.05.006.

[31] S. Tao, J.T.S. Irvine, A redox-stable efficient anode for solid-oxide fuel cells, Nat. Mater. 2 (2003) 320–323. https://doi.org/10.1038/nmat871.

[32] J.C. Ruiz-Morales, D. Marrero-López, J. Canales-Vázquez, J.T.S. Irvine, Symmetric and reversible solid oxide fuel cells, RSC Adv. 1 (2011) 1403. https://doi.org/10.1039/c1ra00284h.

[33] S.P. Jiang, L. Zhang, C.S. Cheng, L. Zhang, Development of (La0.75Sr0.25)(Cr0.5Mn0.5)O3 Cathodes of Solid Oxide Fuel Cells by Gelcasting Technique, ECS Trans. 7 (2007) 1081–1088. https://doi.org/10.1149/1.2729205.

[34] C.M. Chanquía, J.E. Vega-Castillo, A.L. Soldati, H. Troiani, A. Caneiro, Synthesis and characterization of pure-phase La0.75Sr0.25Cr0.5Mn0.5O3−δ nanocrystallites for solid oxide fuel cell applications, J. Nanoparticle Res. 14 (2012) 1104. https://doi.org/10.1007/s11051-012-1104-1.

[35] A. Caneiro, P. Bavdaz, J. Fouletier, J.P. Abriata, Adaptation of an electrochemical system for measurement and regulation of oxygen partial pressure to a symmetrical thermogravimetric analysis system developed using a Cahn 1000 electrobalance, Rev. Sci. Instrum. 53 (1982) 1072–1075. https://doi.org/10.1063/1.1137090.

[36] T. Delahaye, T. Jardiel, O. Joubert, R. Laucournet, G. Gauthier, M.T. Caldes, Electrochemical properties of novel SOFC dual electrode La0.75Sr0.25Cr0.5Mn0.3Ni0.2O3−δ□, Solid State Ionics. 184 (2011) 39–41. https://doi.org/10.1016/j.ssi.2010.10.015.

[37] A. Nenning, L. Volgger, E. Miller, L. V. Mogni, S. Barnett, J. Fleig, The Electrochemical Properties of Sr(Ti,Fe)O 3-δ for Anodes in Solid Oxide Fuel Cells,

J. Electrochem. Soc. 164 (2017) F364–F371. https://doi.org/10.1149/2.1271704jes.

[38] P.K. Dager, L.V. Mogni, S. Soria, A. Caneiro, High temperature properties of Sr2MgMo0.9TM0.1O6−δ (TM = Mn, Co and Ni), Ceram. Int. 44 (2018) 2539–2546. https://doi.org/10.1016/j.ceramint.2017.11.006.

[39] D. Marrero-López, J. Peña-Martínez, J.C. Ruiz-Morales, D. Pérez-Coll, M.A.G. Aranda, P. Núñez, Synthesis, phase stability and electrical conductivity of Sr2MgMoO6− anode, Mater. Res. Bull. 43 (2008) 2441–2450. https://doi.org/10.1016/j.materresbull.2007.07.032.

[40] Z. Xie, H. Zhao, Z. Du, T. Chen, N. Chen, X. Liu, S.J. Skinner, Effects of Co Doping on the Electrochemical Performance of Double Perovskite Oxide Sr 2 MgMoO 6−δ as an Anode Material for Solid Oxide Fuel Cells, J. Phys. Chem. C. 116 (2012) 9734–9743. https://doi.org/10.1021/jp212505c.

[41] Z. Xie, H. Zhao, Z. Du, T. Chen, N. Chen, Electrical, Chemical, and Electrochemical Properties of Double Perovskite Oxides Sr 2 Mg 1– x Ni x MoO 6−δ as Anode Materials for Solid Oxide Fuel Cells, J. Phys. Chem. C. 118 (2014) 18853–18860. https://doi.org/10.1021/jp502503e.

[42] S.B. Adler, Factors Governing Oxygen Reduction in Solid Oxide Fuel Cell Cathodes, Chem. Rev. 104 (2004) 4791–4844. https://doi.org/10.1021/cr020724o.

[43] M.M. Kuklja, E.A. Kotomin, R. Merkle, Y.A. Mastrikov, J. Maier, Combined theoretical and experimental analysis of processes determining cathode performance in solid oxide fuel cells, Phys. Chem. Chem. Phys. 15 (2013) 5443. https://doi.org/10.1039/c3cp44363a.

[44] V. KHARTON, E. TSIPIS, I. MAROZAU, A. VISKUP, J. FRADE, J. IRVINE, Mixed conductivity and electrochemical behavior of

(La0.75Sr0.25)0.95Cr0.5Mn0.5O3−δ, Solid State Ionics. 178 (2007) 101–113. https://doi.org/10.1016/j.ssi.2006.11.012.

[45] T. Zhu, D.E. Fowler, K.R. Poeppelmeier, M. Han, S.A. Barnett, Hydrogen Oxidation Mechanisms on Perovskite Solid Oxide Fuel Cell Anodes, J. Electrochem. Soc. 163 (2016) F952–F961. https://doi.org/10.1149/2.1321608jes.

[46] S. McIntosh, M. van den Bossche, Influence of lattice oxygen stoichiometry on the mechanism of methane oxidation in SOFC anodes, Solid State Ionics. 192 (2011) 453–457. https://doi.org/10.1016/j.ssi.2010.07.019.

[47] Klaus-Dieter Kreuer, ed., Fuel Cells Selected Entries from the Encyclopedia of Sustainability Science and Technology, Springer New York, 2013. https://link.springer.com/book/10.1007/978-1-4614-5785-5.

Journal Pre-proof

Journal Pre-proof

Figure Captions

Fig. 1. (a) Arrhenius plot of total conductivity of LSCM in Air and 10%H_2/Ar dry atmospheres and (b) SEM image of the sintered LSCM-bar.

Fig. 2. SEM images of electrode/electrolyte interface (a), top view (b) and XRD pattern (c) of LSCM-electrode surface, after "quick-stuck" thermal treatment at 1000 °C during 10 min.

Fig. 3. (a) Nyquist and (b) Bode plot of EIS spectra collected for the LSCM symmetrical cell collected at 700 ºC by varying the pO_2; (c) log-log plot of the electrode polarization resistance contributions as a function of the pO_2. The n value refers to the $(pO_2)^n$ dependence of polarization resistances.

F**ig. 4.** (a) Nyquist and (b) Bode plot of EIS spectra of the symmetrical cell collected at 700 ºC by varying the pH_2; (c) log-log plot of the electrode polarization resistance contributions as a function of the pH_2. The n value refers to the $(pO_2)^n$ dependence of polarization resistances.

Fig. 5. Schematic illustration of the (a) O_2 reduction and (b) H_2 oxidation on a mixed-conducting oxide electrode, including: O_2 or H_2 gas diffusion, O_2 or H_2 dissociative adsorption on the oxide electrode surface; charge transfer reaction forming O-ion or H_2O molecule; desorption of H_2O from the oxide surface; and oxygen ion diffusion.

Journal Pre-proof

Table 1. Electrochemical and conductivity data obtained for LSCM from the fitting of the EIS spectra with the electrical equivalent circuit (ECC) as a function of pO_2 and pH_2

	Conductivity			Electrode Polarization Impedance					
	Electrical @700 °C		Ionic @950°C[(b)]	High Frequency (Z_{HF})			Low Frequency (Z_{LF})		
	σ_{el}[(a)] (Scm^{-1})	E_a (eV)	σ_O x10^5 (Scm^{-1})	n[(c)]	R_{HF}[(d)] (Ωcm^2)	C_{HF} (Fcm^{-2})	n[(c)]	R_{LF}[(d)] (Ωcm^2)	C_{LF}[(e)] (Fcm^{-2})
Cathode Ar-O_2	8.95	0.19	3	~ 0	5.3(5)	0.05[(d)]	0.37	1.9(1)	0.037(4)
Anode Ar-H_2	0.32	0.44	~ 30	~ 0	23.7(7)	0.001	0.37	39.3(8)	0.0087(2)

a) Data evaluated at 700 °C and pO_2 = 0.21 atm (cathode) or pH_2 ~0.1 atm (anode).

b) From ref. [44]

c) n from pO_2^{-n} or pH_2^{-n}

d) Average polarization resistance.

e) Pseudo-capacitance o chemical capacitance of Warburg-type impedance $C_W = \frac{\sqrt{W_{-T}}}{R_W}$

Journal Pre-proof

Journal Pre-proof

Journal Pre-proof

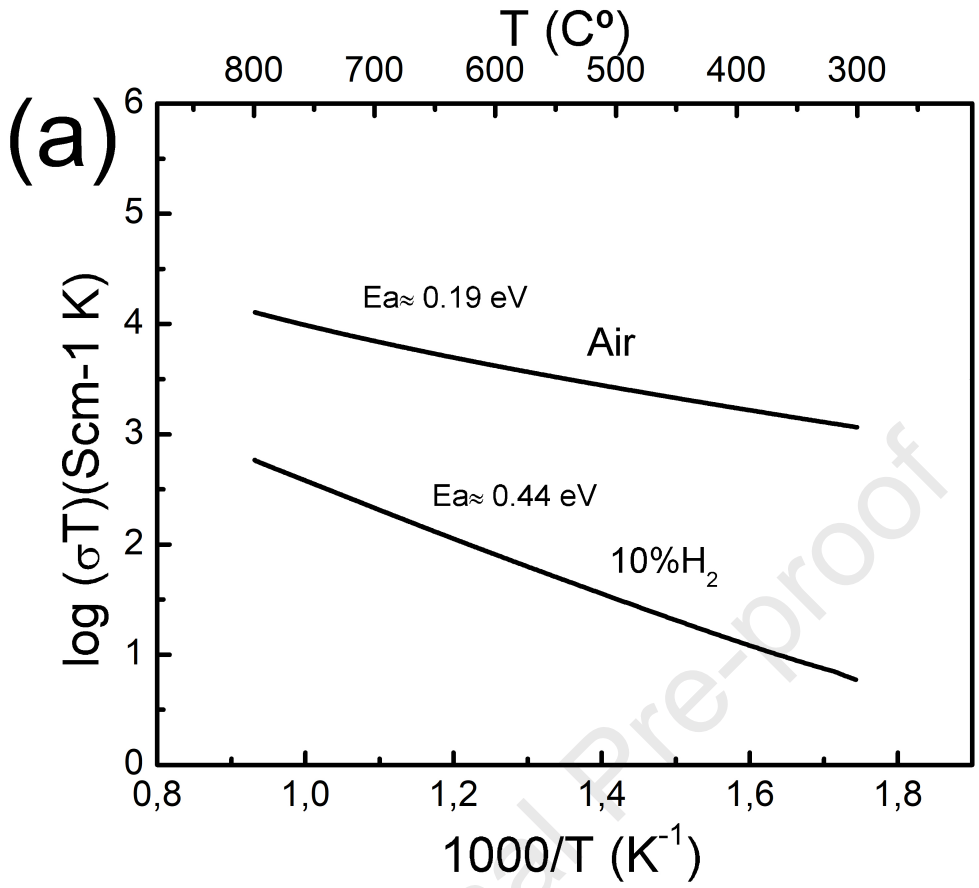

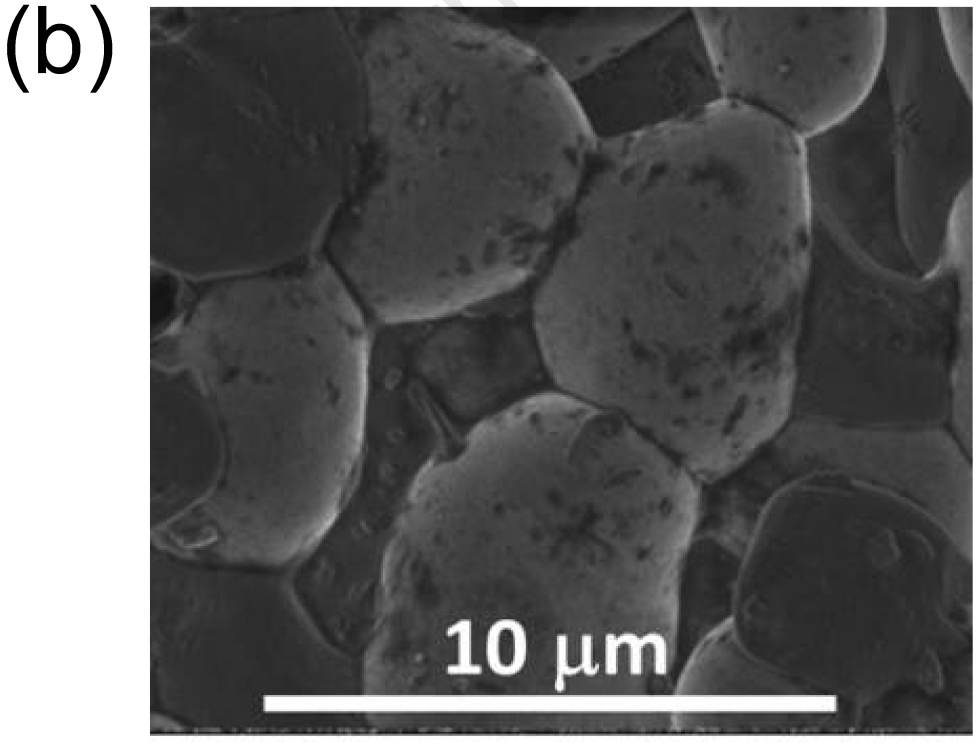

Journal Pre-proof

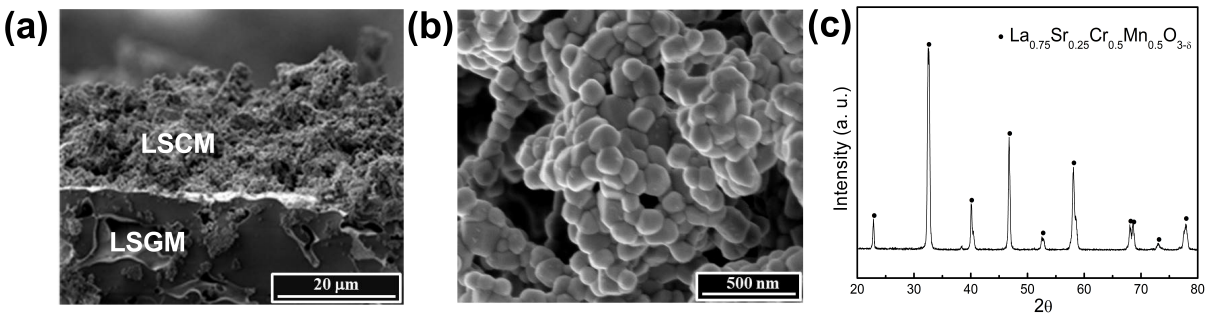

Journal Pre-proof

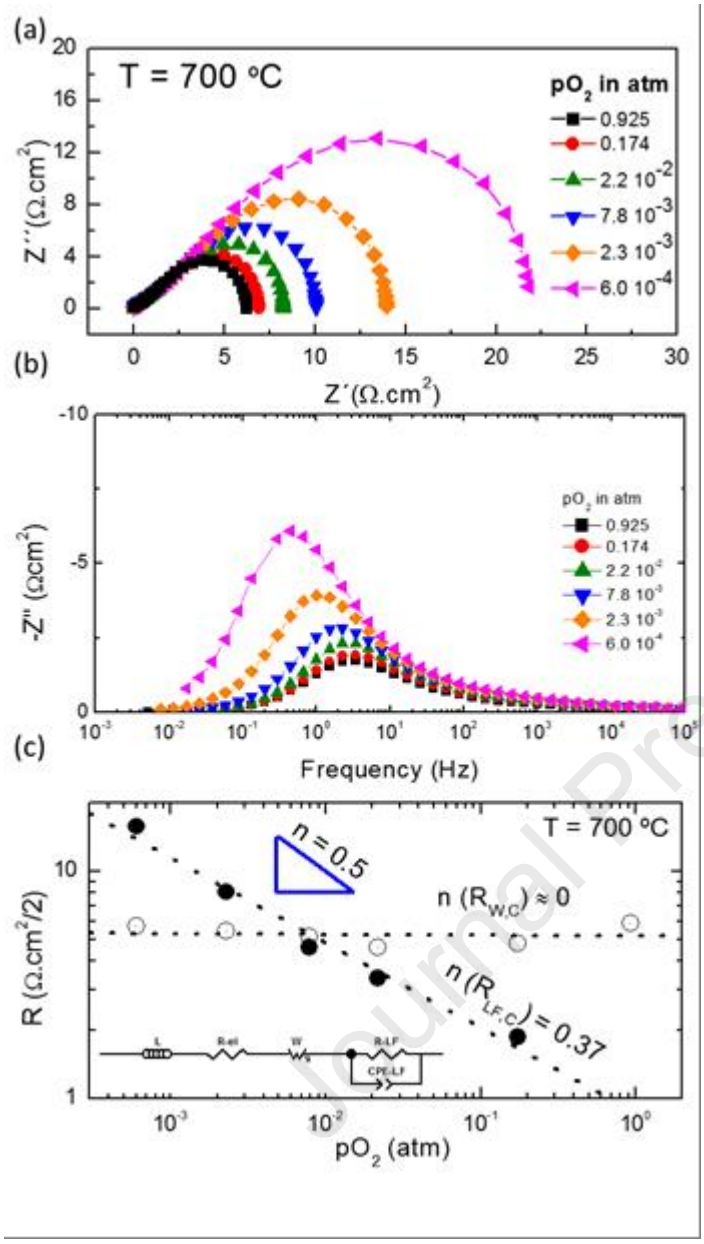

Journal Pre-proof

(a)

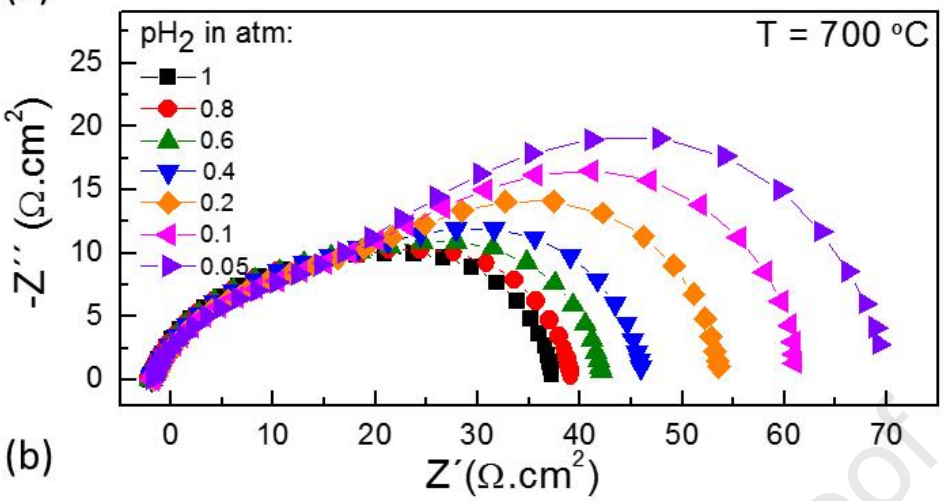

(b)

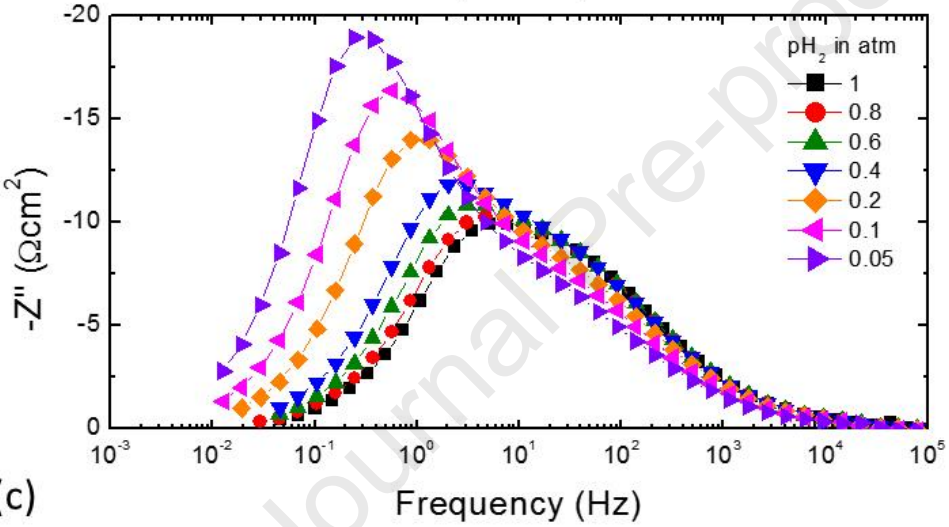

(c)

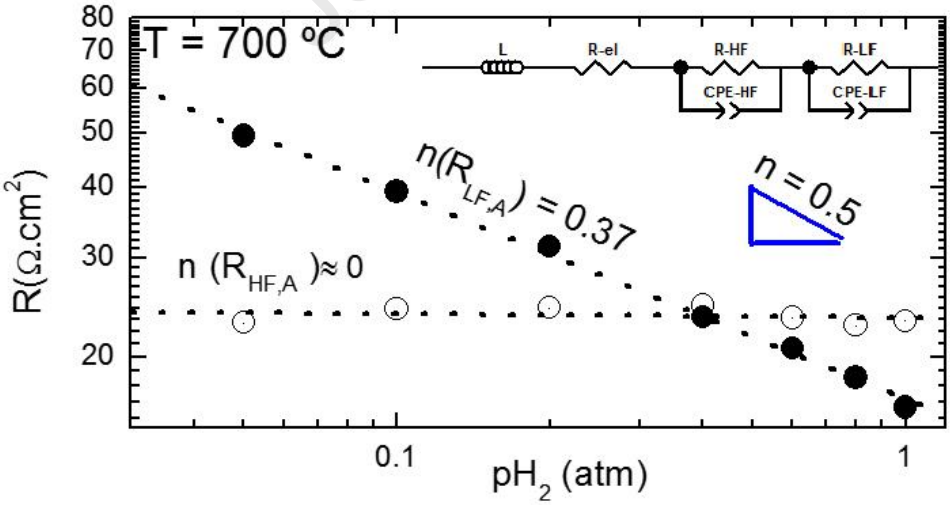

Journal Pre-proof

(a) O_2 reduction

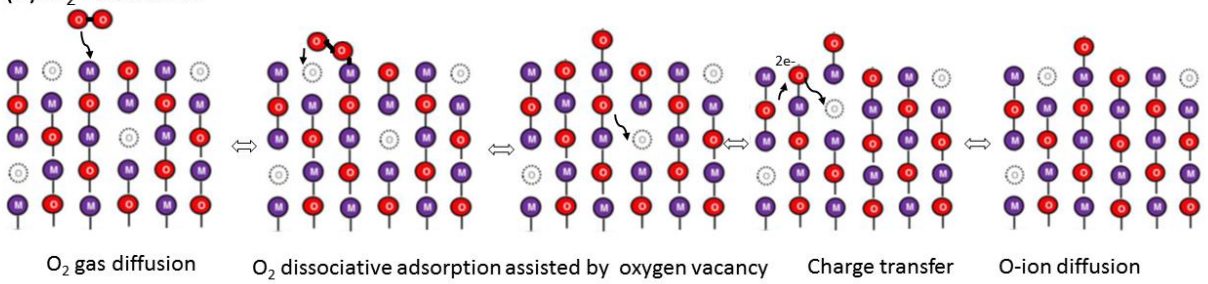

(b) H_2 oxidation

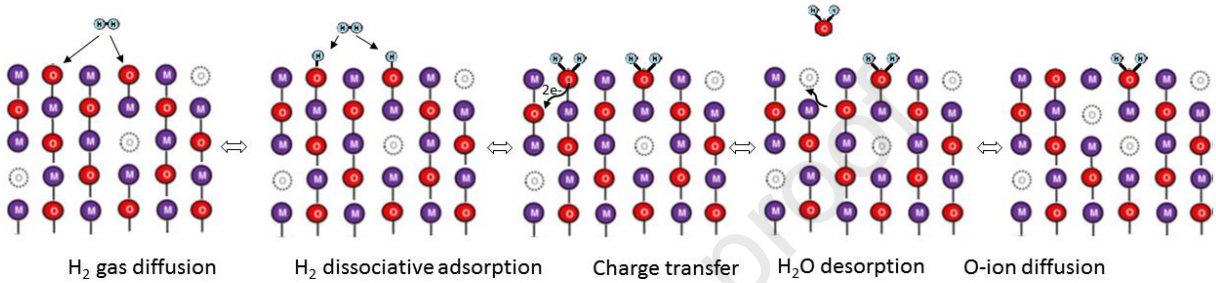

Journal Pre-proof

Journal Pre-proof

Declaration of interests

☒ The authors declare that they have no known competing financial interests or personal relationships that could have appeared to influence the work reported in this paper.

☐The authors declare the following financial interests/personal relationships which may be considered as potential competing interests:

We don't have financial interests/personal relationships

Journal Pre-proof